Supporting Information

Preparation of Non-heme {FeNO}^{7} Models of Cysteine Dioxygenase: Sulfur versus Nitrogen Ligation and Photorelease of Nitric Oxide

Alison C. McQuilken,[†] Yang Ha,[§] Kyle D. Sutherlin,[§] Maxime A. Siegler,[†] Keith O. Hodgson,[§,⊥] Britt Hedman,[⊥] Edward I. Solomon,*[,§] Guy N. L. Jameson,*[,‡] and David P. Goldberg*[,†]

†Department of Chemistry, The Johns Hopkins University, Baltimore, Maryland, 21218, United States

‡Department of Chemistry and MacDiarmid Institute for Advanced Materials and Nanotechnology, University of Otago, P.O. Box 56, Dunedin 9054, New Zealand

§Department of Chemistry, Stanford University, Stanford, California 94305, United States

⊥Stanford Synchrotron Radiation Lightsource, SLAC, Stanford University, Menlo Park, California 94025, United States

I. General Procedures. All reagents were purchased from commercial vendors and used without further purification unless otherwise noted. Diethyl ether and dichloromethane were purified via a Pure-Solv Solvent Purification System from Innovative Technology, Inc. Methanol and acetonitrile were distilled over CaH_2. All solvents were degassed by repeated cycles of freeze-pump-thaw and stored in an N_2-filled drybox. Nitric oxide gas was purchased from Matheson gases and purified according to a literature procedure[1] and was stored in a sealed Schlenk flask until use. $^{15}N^{18}O$(g) (98 atom % ^{15}N, 95 atom % ^{18}O) was purchased from Sigma Aldrich and used without further purification. The iron(II) starting material, $[Fe^{II}(N3PyS)(CH_3CN)]BF_4$ (**1**), was synthesized according to a literature procedure.[2]

II. Physical Methods. UV-visible spectra were recorded on a Hewlett-Packard 8542 photodiode-array spectrophotometer equipped with HPChemstation software. ^1H NMR spectra were recorded on a Bruker Avance 400 MHz FT-NMR spectrometer at 25 ºC. Elemental analysis was performed by Atlantic Microlab Inc., Norcross, GA. Cyclic voltammetry for **3** in CH_3CN and **4** in CH_3OH was measured with an EG&G Princeton Applied Research potentiostat/galvanostat model 263A with a three-electrode system consisting of a glassy carbon working electrode, a $Ag/AgNO_3$ non-aqueous reference electrode (0.01 M $AgNO_3$ in CH_3CN with 0.1 M $TBAPF_6$), and a platinum wire counter electrode. Measurements were performed with 0.10 M tetrabutylammonium hexafluorophosphate ($TBAPF_6$) as the supporting electrolyte (purchased from Sigma Aldrich, recrystallized from ethanol, and dried under vacuum prior to use) in dry CH_3CN or CH_3OH at ambient temperatures under an atmosphere of N_2. Potentials were calculated from $E_{1/2} = (E_{pa} + E_{pc})/2$ and were referenced to the ferrocenium/ferrocene couple (Fc^+/Fc). Positive mode electrospray ionization mass spectra (ESI-MS) were collected on

a Thermo Finnigan LCQ Duo ion-trap mass spectrometer fitted with an electrospray ionization source. The spray voltage was set at 5 kV and the capillary temperature was held at 250 °C. Attenuated total reflectance (ATR) infrared spectra of neat crystalline material were obtained with a Golden Gate Reflectance diamond cell in a Nexus 670 Thermo-Nicolet FTIR spectrometer. Solution IR spectra were obtained using Spectralys Specac solution IR cell fit with CaF_2 salt plates and capped. Electron paramagnetic resonance (EPR) spectroscopy experiments were performed on a Bruker EMX spectrometer controlled with a Bruker ER 041 X G microwave bridge and equipped with a continuous-flow liquid helium cryostat (ESR900) coupled to an Oxford Instruments TC503 temperature controller. The spectra were obtained at 14 K under nonsaturating microwave power conditions (ν = 9.475 GHz, microwave power = 0.201 mW, modulation amplitude = 10 G, modulation frequency = 100 kHz). EPR simulations were conducted using WinEPR SimFonia software version 1.26, 1997. Mössbauer spectra were recorded on a spectrometer from SEE Co. (Science Engineering & Education Co., MN) equipped with a closed cycle refrigerator system from Janis Research Co. and SHI (Sumitomo Heavy Industries Ltd.). Approximately 10 mg of sample was mixed in a sucrose support and placed in a custom sample holder made from Teflon and specifically designed for solid samples. Data were collected in constant acceleration mode in transmission geometry with an applied field of 47 mT parallel to the γ-rays. The zero velocity of the Mössbauer spectra refers to the centroid of the room temperature spectrum of a 25 μm metallic iron foil. Analysis of the spectra was conducted using the WMOSS program (SEE Co., formerly WEB Research Co., Edina, MN).

III. Synthesis

$[Fe^{II}(N4Py)(CH_3CN)](BF_4)_2$ (2). Following a literature procedure,[3] N4Py (180 mg, 0.5 mmol) was dissolved in CH_3CN/CH_3OH (1:1, 2 mL) and added dropwise to $Fe^{II}(BF_4)_2 \bullet 6H_2O$ (140 mg, 0.42 mmol) dissolved in CH_3CN/CH_3OH (1:1, 2 mL) in a dry box. The solution was stirred for 30 min, filtered through Celite, and slow vapor diffusion of diethyl ether resulted in isolation of dark red crystals of **2**. ^{1}H NMR (CD_3CN): δ 9.01 (d, 2 H, J = 5.5 Hz, py), 8.88 (d, 2 H, J = 5.5 Hz, py), 7.90 (m, 4 H, py), 7.66 (m, 2 H, py), 7.33 (m, 4 H, py), 7.04 (d, 2 H, J = 7.8 Hz, py) 6.31 (s, 1 H, CH), 4.36 (d, 2 H, J = 18.0 Hz, CH_2), 4.26 (d, 2 H, J = 18.0 Hz, CH_2).

$[Fe(NO)(N3PyS)]BF_4$ (3). An amount of $[Fe^{II}(N3PyS)(CH_3CN)]BF_4$ (15 mg, 0.025 mmol) was dissolved in CH_3CN (3 mL) in a Schlenk flask sealed with a rubber septum, after which excess NO(g) (8 mL) was injected into the solution. The color of the solution immediately changed from red to brown, and the solution was then allowed to stir for an additional 30 min. Removal of the excess NO(g) and all volatiles *in vacuo* resulted in a brown residue, which was then transferred to a dry box and dissolved in CH_2Cl_2 (2 mL) to give a brown solution. The solution was filtered through Celite, and slow vapor diffusion of diethyl ether for 12 h resulted in the precipitation of a brown solid, which was isolated by decanting the mother liquor to give pure **3** (74%). X-ray quality crystals were obtained by dissolving **3** in methanol followed by vapor diffusion of diethyl ether to give **3** as dark brown blocks. Selected IR bands (ATR), ν (cm^{-1}): 1753 (m), 1660 (m), 1606 (m), 1586 (w), 1465 (m), 1442 (m), 1296 (w), 1283 (w), 1053 (s), 1014 (s), 757 (s). ESI-MS: calcd for $[FeC_{24}H_{21}N_5OS]^+$, 483.08; found, 482.6. UV-vis (CH_3CN): λ = 350 nm (ε = 5300 M^{-1} cm^{-1}), 440 nm (ε = 2400 M^{-1} cm^{-1}), 540 nm (ε = 970 M^{-1} cm^{-1}). *Anal. Calcd* for $C_{24}H_{21}N_5OSBF_4Fe$: C, 50.56; H, 3.71; N, 12.28. Found: C, 50.30; H, 3.66; N, 12.02.

[Fe(NO)(N4Py)](BF$_4$)$_2$ (4). An amount of [Fe^{II}(N4Py)(CH$_3$CN)](BF$_4$)$_2$ (12.7 mg, 0.02 mmol) was dissolved in CH$_3$OH (3 mL) in a Schlenk flask sealed with a rubber septum, after which excess NO(g) (8 mL) was injected into the solution. The color of the solution changed from orange to pink, and the solution was allowed to stir for an additional 30 min. The headspace of the reaction flask was evacuated, but care was taken not to bring the solution to dryness, as it was found that **4** was not stable enough to be brought to dryness under vacuum. The reaction flask was then transferred into a dry box. X-ray quality crystals were obtained by slow vapor diffusion of diethyl ether into the methanolic solution, giving **4** as orange-red plates (49%). Selected IR bands (ATR), ν (cm^{-1}): 1672 (m, ν_{NO}), 1609 (m), 1467 (m), 1444 (m), 1293 (w), 1165 (w), 1029 (s), 967 (m), 908 (m), 765 (s). UV-vis (CH$_3$OH): λ = 400 nm (ε = 2200 M^{-1} cm^{-1}), 490 nm (ε = 1600 M^{-1} cm^{-1}). *Anal. Calcd* for C$_{23}$H$_{21}$N$_6$OB$_2$F$_8$Fe•CH$_3$OH: C, 43.74: H, 3.82; N, 12.75. Found: C, 43.27; H, 3.46; N, 12.70.

IV. Experimental Details

Photoirradiation of 3. A solution of **3** (0.1 mM) in CH$_3$CN was loaded into a quartz cuvette (1 cm pathlength) and sealed with a rubber septum. The cuvette was clamped inside the UV-vis spectrophotometer such that spectra could be collected during the photoirradiation experiment. A halogen lamp (150 W) was positioned at a distance of 12 cm from the quartz cuvette ~90° to the UV-vis beam, with a 400 nm long-pass filter placed between the cuvette and the lamp. The photoirradiation was initiated and maintained for 45 min. The spectrum for **3** converted to that observed for **1** as shown in Figure 3. Once the photorelease of NO• from **3** was completed, the halogen lamp was switched off and the rebinding of NO• was observed by UV-vis over 6.5 h (Figure S10).

Photoirradiation of 4. A solution of **4** (0.2 mM) in CH_3OH was loaded into a quartz cuvette (1 cm pathlength) and sealed with a rubber septum. The cuvette was clamped inside the UV-vis spectrophotometer such that spectra could be collected during the photoirradiation experiment. A halogen lamp (150 W) was positioned at a distance of 12 cm from the quartz cuvette ~90° to the UV-vis beam, with a 400 nm long-pass filter placed between the cuvette and the lamp. The photoirradiation was initiated and maintained for 100 min. A UV-vis spectrum was obtained every 5 min, and minimal changes were observed during photoirradiation (Figure S12).

V. X-Ray Crystallography. All reflection intensities were measured at 110(2) K using a KM4/Xcalibur (detector: Sapphire3) with enhance graphite-monochromated Mo *K*α radiation (λ = 0.71073 Å) under the program CrysAlisPro (Version 1.171.35.11 Oxford Diffraction Ltd., 2011). The program CrysAlisPro (Version 1.171.35.11, Oxford Diffraction Ltd., 2011) was used to refine the cell dimensions. Data reduction was done using the program CrysAlisPro (Version 1.171.35.11, Oxford Diffraction Ltd., 2011). The structures were solved with the program SHELXS-97[4] and were refined on F^2 with SHELXL-97.[4] Analytical numeric absorption corrections based on a multifaceted crystal model were applied using CrysAlisPro (Version 1.171.35.11, Oxford Diffraction Ltd., 2011). The temperature of the data collection was controlled using the system Cryojet (manufactured by Oxford Instruments). The H atoms (except when specified) were placed at calculated positions using the instruction AFIX 13, AFIX 23, AFIX 43, AFIX 137 or AFIX 147 (the latter instruction was exclusively used for the refinement of **4**) with isotropic displacement parameters having values 1.2 or 1.5 times *U*eq of the attached C or O atoms.

Crystal Structure of 2. The structure of **2** is partially disordered; the two counterions are disordered over two orientations, and the the major components of the disorder refine to about 0.664(17) and 0.894(3). A first refinement against F^2 was not satisfactory because some residual electron density was found in four small voids located at (0 0 0), (0 ½ 0), (½ 0 ½), (½ ½ ½), which include 19 electrons in a volume of 58-71 Å^3. Each void most likely contains one molecule of disordered solvent methanol molecule (the solvent molecules are always found to be disordered over two orientations via inversion symmetry). Their contributions were taken out for the subsequent stages of the refinement using the program SQUEEZE.

2: Fw = 637.97,* dark red block, 0.39 × 0.29 × 0.23 mm^3, monoclinic, $P2_1/n$ (no. 14), a = 12.08096(14), b = 18.3226(2), c = 12.90108(15), β = 94.6216(10)°, V = 2846.43(6) Å^3, Z = 4, D_x = 1.489 g cm^{-3},* μ = 0.609 mm^{-1},* abs. corr. range: 0.839–0.904. 26665 Reflections were measured up to a resolution of $(\sin \theta/\lambda)_{max}$ = 0.65 Å^{-1}. 6531 Reflections were unique (R_{int} = 0.0371), of which 5464 were observed [$I > 2\sigma(I)$]. 460 Parameters were refined with 254 restraints. $R1/wR2$ [$I > 2\sigma(I)$]: 0.0386/0.1004. $R1/wR2$ [all refl.]: 0.0470/0.1041. S = 1.067. Residual electron density found between −0.47 and 0.71 e Å^{-3}.

*excluding the contribution of unresolved residual electron density

Crystal Structure of 3. The nitric oxide and the BF_4^- counterions are found to be disordered over two orientations, and the major components of the disorder refine to about 0.886(10) and 0.597(6), respectively.

3: Fw = 570.18, black block, 0.56 × 0.42 × 0.29 mm^3, orthorhombic, *Pbca* (no. 61), a = 11.65041(18), b = 14.6344(2), c = 28.0712(5) Å, V = 4786.05(13) Å^3, Z = 8, D_x = 1.583 g cm^{-3}, μ = 0.778 mm^{-1}, abs. corr. range: 0.714–0.832. 19130 Reflections were measured up to a

resolution of (sin $\theta/\lambda)_{max}$ = 0.65 Å^{-1}. 5498 Reflections were unique (R_{int} = 0.0272), of which 4680 were observed [$I > 2\sigma(I)$]. 390 Parameters were refined using 163 restraints. $R1/wR2$ [$I > 2\sigma(I)$]: 0.0364/0.0908. $R1/wR2$ [all refl.]: 0.0447/0.0948. S = 1.037. Residual electron density found between -0.480 and 0.746 e Å^{-3}.

Crystal Structure of 4. Crystals used for X-ray analysis were obtained by reaction of **2** with excess $NO_{(g)}$ in CH_2Cl_2, which resulted in precipitation. Recrystallization in CH_3OH/Et_2O afforded X-ray quality crystals of **4**. Unit cell measurements for different batches of crystals of **4** grown by the routine procedure described above, which avoids the use of CH_2Cl_2, matched that found for the original structure of **4**.

The asymmetric unit contains one ordered Fe complex, one ordered and one disordered BF_4^- counterions (disordered over 3 orientations; the three different orientations have occupancy factors of 0.394(6), 0.259(3) and 0.240(6); their sum is not equal to one due to the Cl^- contamination, see below for further details), and one disordered lattice (*i.e.*, uncoordinated) MeOH solvent molecule (disordered over 2 orientations; the major component of the disorder refines to 0.781(9)). The H atom attached to the OH group of the minor component could not be located. At sites in which the BF_4^- counterions are found in the crystal lattice, there seem to be some residual amounts of Cl^- contamination (the two Cl atoms are located near the B atom positions). The occupancy factors of the two sites BF_4^-/Cl^- were refined freely using free variables, and their values are 0.923(2)/0.077(2) are 0.893(5)/0.107(3).

4: Fw = 649.64, orange-red plate, 0.29 × 0.26 × 0.06 mm^3, orthorhombic, $Pna2_1$ (no. 33), a = 17.0215(3), b = 12.70711(18), c = 12.66693(19) Å, V = 2739.78(7) Å^3, Z = 4, D_x = 1.575 g cm^{-3}, μ = 0.653 mm^{-1}, abs. corr. range: 0.861–0.968. 18464 Reflections were measured up to a

resolution of $(\sin \theta/\lambda)_{max}$ = 0.62 Å^{-1}. 5214 Reflections were unique (R_{int} = 0.0349), of which 4802 were observed [$I > 2\sigma(I)$]. 476 Parameters were refined using 544 restraints. $R1/wR2$ [$I > 2\sigma(I)$]: 0.0319/0.0820. $R1/wR2$ [all refl.]: 0.0369/0.0839. S = 1.024. Residual electron density found between −0.48 and 0.47 e Å^{-3}.

VI. S K-edge X-ray Absorption Spectroscopy Data Collection and Analysis*

Sulfur K-edge data were measured at the Stanford Synchrotron Radiation Lightsource beam line 4-3. Details of the beam line configuration have been described previously.[5] The sample was ground into fine powder and dispersed as thinly as possible on a Kapton tape to minimize the possible self-absorption effects of fluorescence. The photon energy was calibrated to the maximum of the first pre-edge feature of $Na_2S_2O_3 \bullet 5H_2O$ at 2472.02 eV. Five scans were measured on the sample to ensure reproducibility. Raw data were calibrated and averaged using MAVE in the EXAFSPAK package.[6] By using the PySpline program,[7] the background was removed from all spectra by fitting a second-order polynomial to the pre-edge region and subtracting it from the entire spectrum. Normalization of the data was accomplished by fitting a straight line to the post-edge region and normalizing the edge jump to 1.0 at 2490.0 eV. The error from background subtraction and normalization is less than 1%. Intensities of the pre-edge features were quantified by fitting the data with pseudo-Voigt line shapes with a fixed 1:1 ratio of Lorentzian to Gaussian contributions, using the EDG_FIT program.[6] The error from the fitting procedure is less than 1%. The fitted intensities were converted to %S 3p character according to the literature.[8]

*This portion of the research was carried out at the Stanford Synchrotron Radiation Lightsource, a Directorate of SLAC National Accelerator Laboratory and an Office of Science User Facility

operated for the U.S. Department of Energy Office of Science by Stanford University. The SSRL Structural Molecular Biology Program is supported by the DOE Office of Biological and Environmental Research, and by the National Institutes of Health, National Institute of General Medical Sciences (including P41GM103393).

VII. Supporting Figures

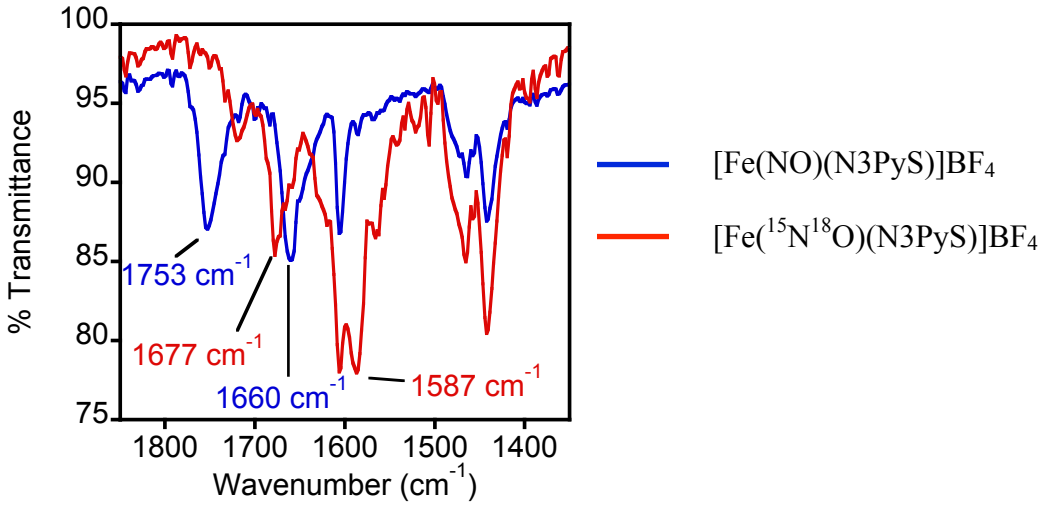

Figure S1. ATR-IR of crystalline **3** (blue) and of crystalline [Fe(^{15}N^{18}O)(N3PyS)]BF_4 (red).

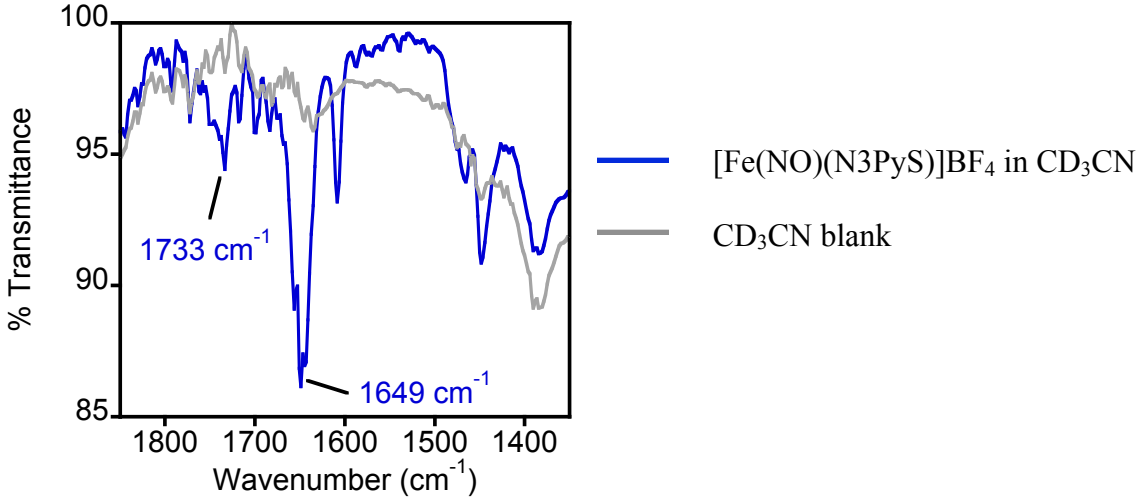

Figure S2. Solution IR spectra of crystalline **3** dissolved in CD_3CN (blue) and of CD_3CN solvent blank (grey).

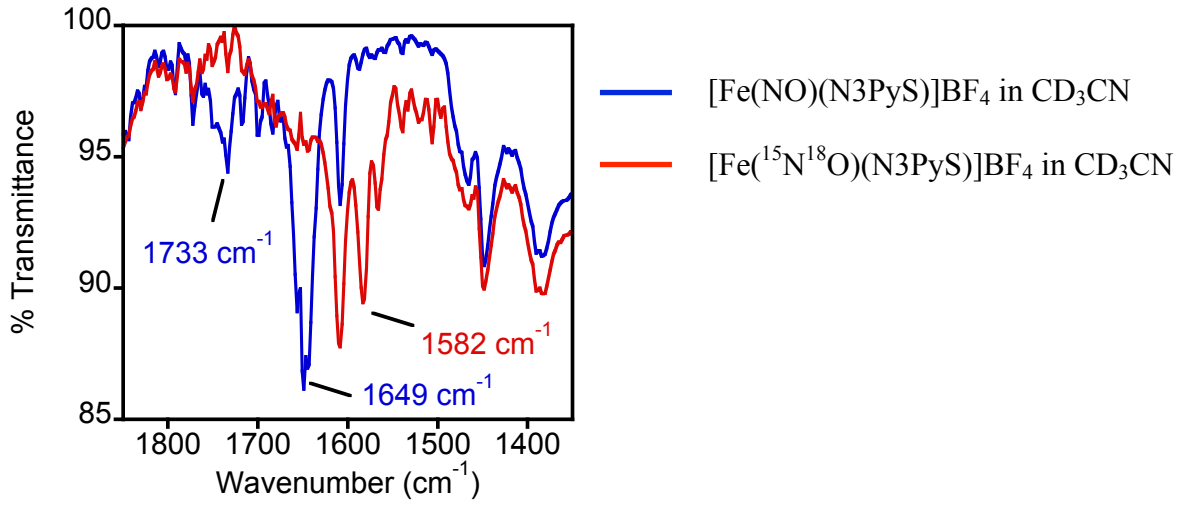

Figure S3. Solution IR spectra of crystalline **3** dissolved in CD_3CN (blue) and of $[Fe(^{15}N^{18}O)(N3PyS)]BF_4$ dissolved in CD_3CN (red).

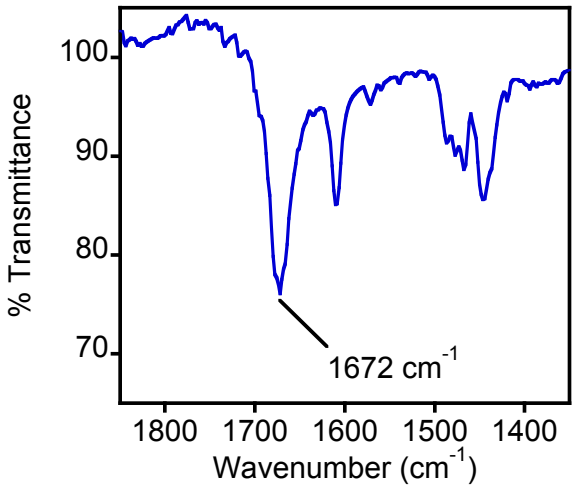

Figure S4. ATR-IR of crystalline **4**.

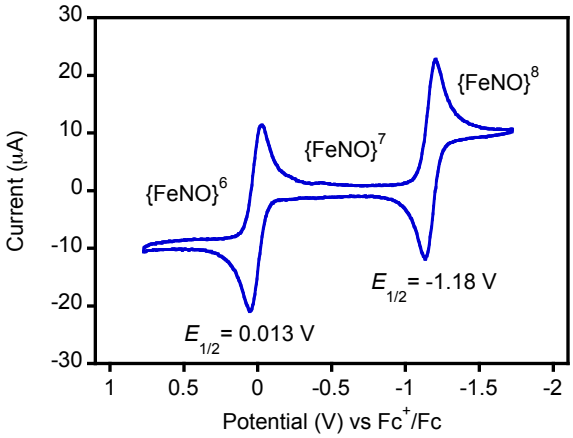

Figure S5. Cyclic voltammogram of a 1.5 mM solution of **3** in CH_3CN with 0.1 M $TBAPF_6$ as supporting electrolyte, scan rate 50 mV/s.

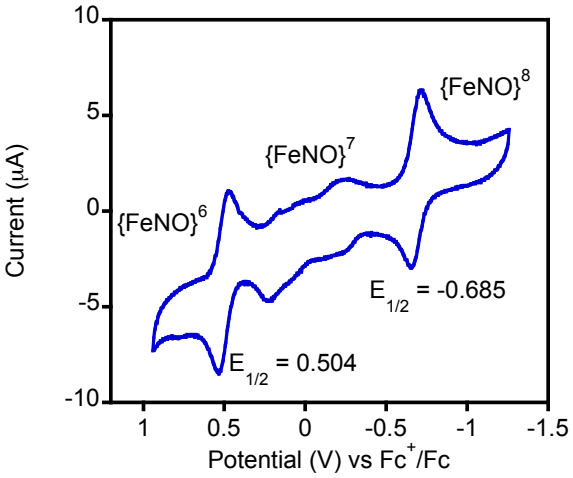

Figure S6. Cyclic voltammogram of a 1.5 mM solution of **4** in CH_3OH with 0.1 M $TBAPF_6$ as supporting electrolyte, scan rate 50 mV/s. The features between -0.25 and 0.25 V are likely due to decomposition of this highly air-sensitive complex during the electrochemical experiment.

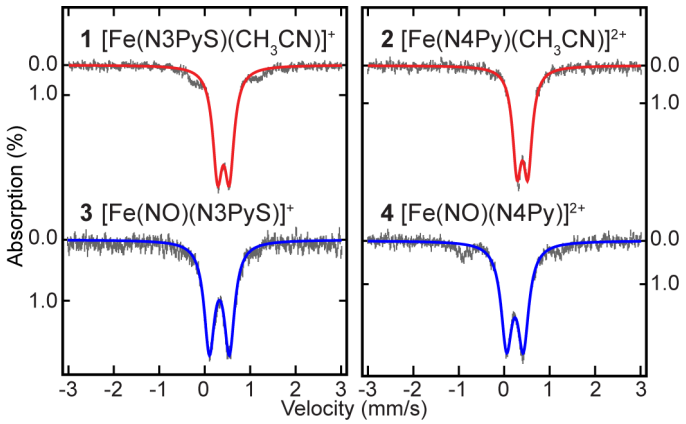

Figure S7. Mössbauer spectra (5.4 K) for solid **1** – **4**.

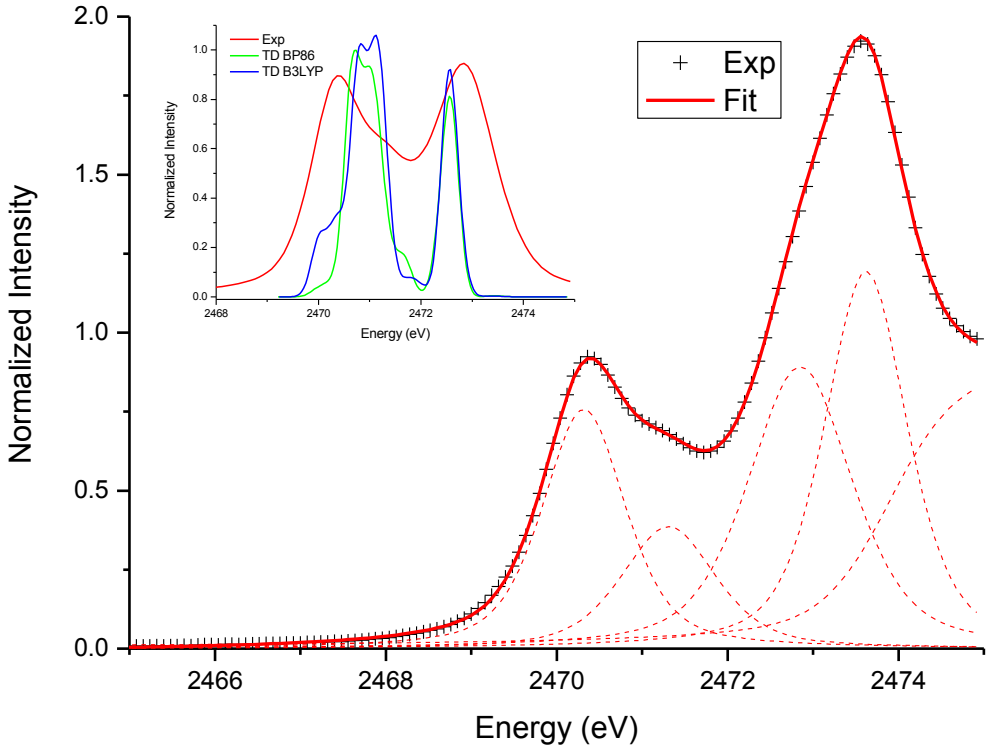

Figure S8. Fits to the S K-edge XAS pre-edge spectral features of complex **3**. Inset: TD calculated spectra vs experiment.

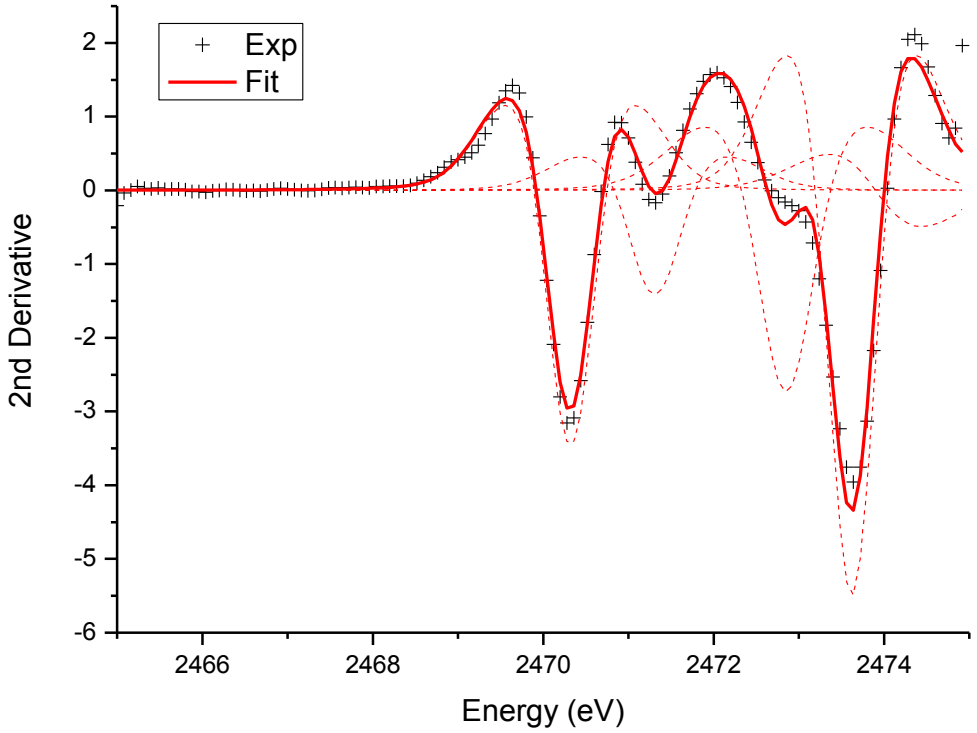

Figure S9. Fits to the 2nd derivative of the S K-edge XAS pre-edge features of complex **3**.

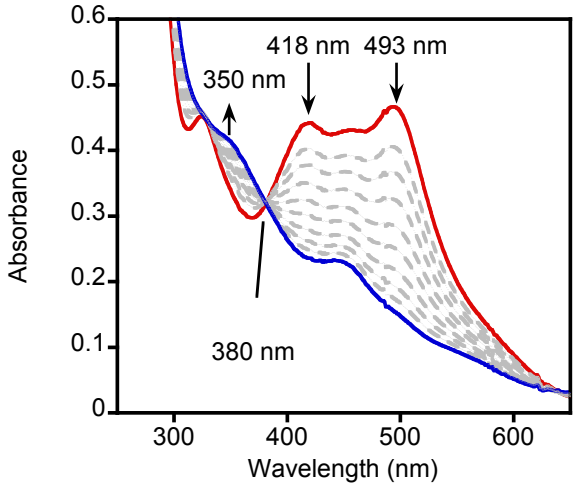

Figure S10. The time-resolved UV-vis spectra (0 – 6.5 h) showing the regeneration of $[Fe(NO)(N3PyS)]^{+}$ (0.1 mM) (blue) from $[Fe^{II}(N3PyS)(CH_3CN]^{+}$ (red) upon removal of the light source in CH_3CN.

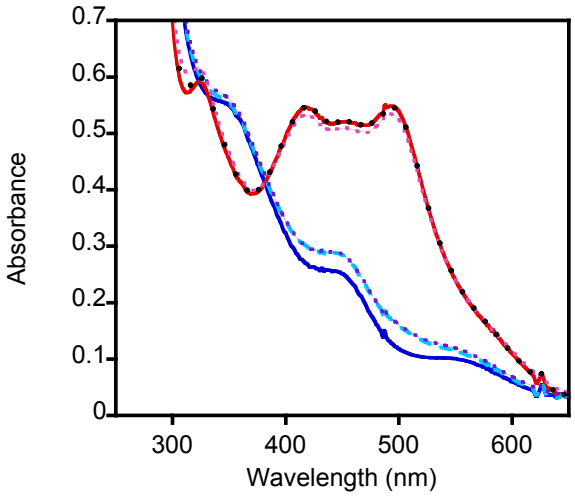

Figure S11. UV-vis spectra of multiple cycles of photodissocation and re-binding of NO for $[Fe(NO)(N3PyS)]^+$ (**3**). Starting from **3** (blue, solid), photoirradiation generates $[Fe^{II}(N3PyS)(CH_3CN)]^+$ (**1**) (red, solid). Removing the light source regenerates **3** (light blue, dashed) and a second photoirradiation regenerates **1** (black, dotted). Removing the light source again gives **3** (purple, dotted) and a third photoirradiation regenerates **1** (pink, dotted).

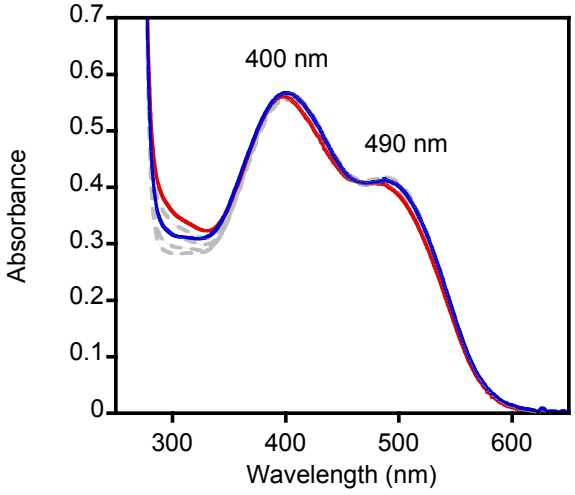

Figure S12. UV-vis spectral changes observed upon continuous photoirradiation ($\lambda > 400$ nm) of **4** (blue) in CH_3OH to final spectrum in red (time = 100 min).

VIII. Computational Studies. DFT calculations with different initial guesses for the spin polarization on Fe and NO were performed using Gaussian 09[9], with both the pure functional BP86 and the hybrid functional B3LYP, and with 6-311G(d) basis sets on Fe, N, O and S, and 6-31G(d) basis sets on C and H. Independent of the initial guess for spin polarization, equivalent final electronic structures were obtained. The geometric structure matches the experimental crystal structure (Table S1). Time-dependent DFT (TD-DFT) calculations were performed on these optimized structures to simulate the S K-edge XAS data, using ORCA, with the CP(PPP) basis set on Fe and the TZVP basis set on the other atoms. Both the B3LYP and BP86 functionals reasonably reproduce the energy splittings and relative intensity of the experimental S K-edge XAS of **3** (Figure S8, insert). The quadrupole splitting and density at the iron nucleus were also obtained using the same basis set and functionals in ORCA. The density at the iron nucleus was converted into an isomer shift using previously-published calibrations.[10,11] The parameters derived from B3LYP (δ = 0.36 mm/s, ΔE_Q = -0.42 mm/s) are in better agreement with experiment than the parameters derived from BP86 (δ = 0.19 mm/s, ΔE_Q = -0.46 mm/s). Since the DFT calculations are in good agreement with experiment, these can be used to describe the electronic structure of the $\{FeNO\}^7$ S = ½ complex **3**. In B3LYP, the spin is mostly localized on the NO (α spin density of NO = 0.7, Fe = 0.3), while with the BP86 functional, the spin is more delocalized (α spin density of NO = 0.4, Fe = 0.6). Both electronic structures are consistent with a ground state consisting mostly of low-spin Fe(II) (S = 0) coupled to NO• (S = ½), with some mixing of low-spin Fe(III) (S = ½) coupled to NO^- (S = 0) character. MO contours and more detailed spin-density information are presented below (Figure S13 and S14, Table S2 and S3).

Scheme S1. Possible electronic structure descriptions for an S = ½ {FeNO}7 complex (a.f. = antiferromagnetically coupled).

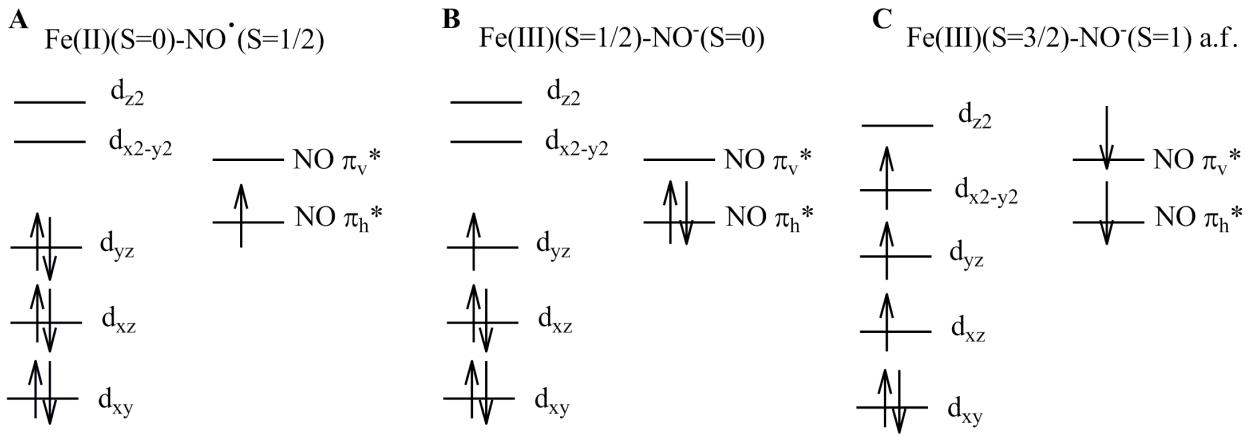

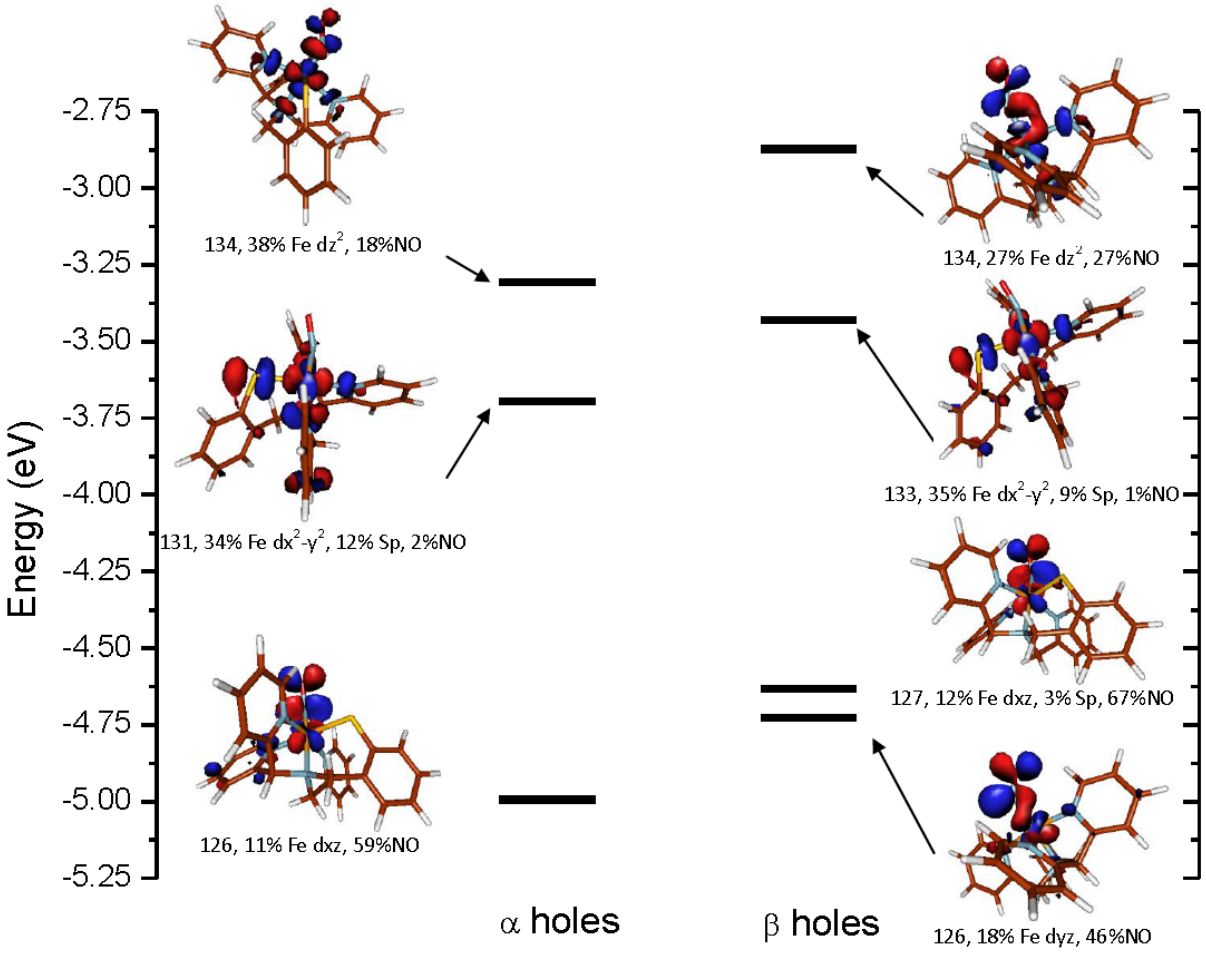

Figure S13. DFT computational energy diagram of complex **3** with the B3LYP functional. The α and β holes reflect uncompensated spin density from the occupied bonding MOs of the complex. α 126 and β 127 form the NO π_v* pair, α 131 and β 133 form the pair of Fe $d_{x^2-y^2}$ orbitals, and α 134 and β 134 form the Fe d_{z^2} pair. The remaining β hole 126 has 18% Fe d_{yz}, and 46% NO contribution, reflecting α-spin localized on the NO with some delocalization onto Fe, as shown in Table S2. This is consistent with a ground state for **3** consisting mostly of low-spin Fe(II) (S = 0) coupled to NO• (S = ½), with some mixing of low-spin Fe(III) (S = ½) coupled to NO^- (S = 0) character (Scheme S1 A and B, respectively).

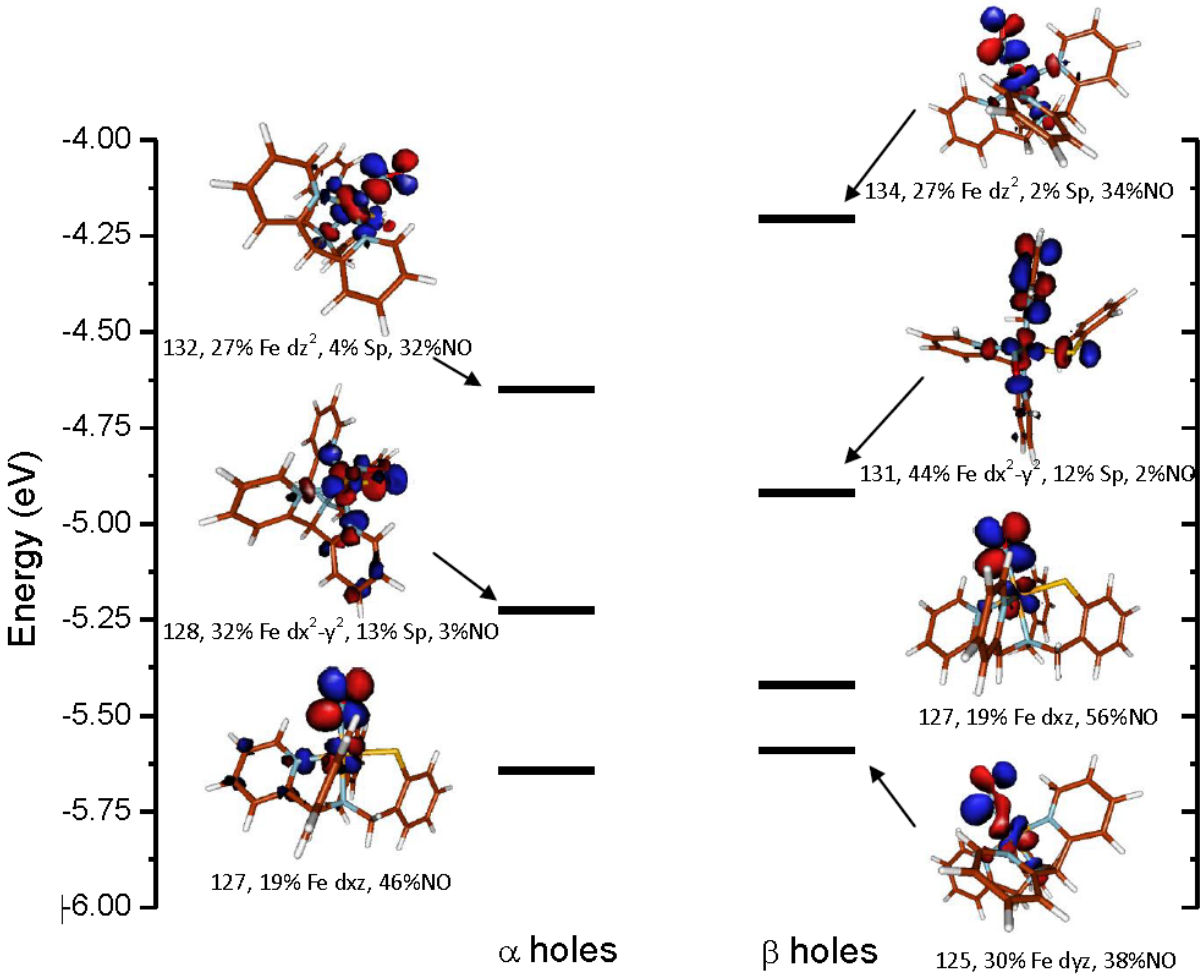

Figure S14. DFT computational energy diagram of complex **3** with the BP86 functional. The α and β holes reflect uncompensated spin density from the occupied bonding MOs of the complex. α 127 and β 127 form the NO π_v* pair, α 128 and β 131 form the pair of Fe $d_{x^2-y^2}$ orbitals, and α 132 and β 134 form the Fe d_{z^2} pair. The remaining unique β hole 125 has 30% Fe d_{yz}, and 38% NO contribution, reflecting α-spin more delocalized between Fe and NO, as shown in Table S3. This reflects an electronic structure description consistent with a ground state consisting of low-spin Fe(II) (S = 0) coupled to NO• (S = ½), with some mixing of low-spin Fe(III) (S = ½) coupled to NO^- (S = 0) character (Scheme S1 A and B, respectively). BP86 predicts a greater delocalization of the α-electron between Fe and NO than B3LYP (Figure S13).

Table S1. DFT optimized geometric structures compared with crystal structure for complex **3**.[a]

	B3LYP	BP86	Exp
	Bond distance (Å)		
Fe-N(NO)	1.75	1.71	1.73
N-O	1.17	1.19	1.15
Fe-S	2.33	2.32	2.30
Fe-N2 (equatorial)	2.01	1.96	1.99
Fe-N3 (equatorial)	2.04	2.00	2.03
Fe-N4 (equatorial)	2.02	2.00	2.01
Fe-N1(trans axial)	2.10	2.13	2.13
	Angle (degree)		
Fe-N-O	144	144	147
S-Fe-NO	89	89	91
(trans axial) N-Fe-NO	177	178	175

[a] In B3LYP, bond lengths agree with the crystallography within 0.03 Å, and angles agree within 3°, while in BP86, bond lengths agree with the crystallography within 0.04 Å, and angles agree within 3°. The N-O bond length derived from B3LYP is closer to experiment than that derived from BP86. Both functionals thus give good quantitative agreement with the crystallography, with B3LYP giving better agreement on the FeNO unit.

Table S2. Computational Spin Density on fragments of complex **3** with B3LYP Functional

	Charge	α Spin
Fe	1.14	0.29
NO	-0.22	0.72
Total on the whole complex	1.00	1.00

Table S3. Computational Spin Density on fragments of complex **3** with BP86 Functional

	Charge	α Spin
Fe	1.09	0.64
NO	-0.25	0.37
Total on the whole complex	1.00	1.00

Cartesian Coordinates:

B3LYP:

Fe	-0.42283100	0.10546200	0.79952700
S	1.11601400	-1.50434200	1.49920600
C	2.40035600	-1.48726300	0.27426400
C	3.74216300	-1.54465700	0.68932900
C	4.77952200	-1.59458300	-0.23970300
C	4.50324600	-1.56965200	-1.60922500
C	3.17762700	-1.50497700	-2.03457000
C	2.12352100	-1.47023800	-1.11191600
C	0.70056000	-1.47190000	-1.59668500
C	-1.48335400	-0.28753100	-1.66355500
C	-2.12482200	-1.39311900	-0.83609700
C	-2.99274500	-2.35656100	-1.33436200
C	-3.53850300	-3.28587100	-0.44503400
C	-3.19059000	-3.21686900	0.90241000
C	-2.30538900	-2.22623800	1.32319900
C	-2.14880700	1.01214700	-1.24531800
C	-3.07426800	1.72612900	-1.99813600
C	-3.62963400	2.88299000	-1.44522800
C	-3.23392700	3.28258900	-0.16892000
C	-2.29598200	2.51363300	0.51674800
C	0.67830400	0.98906200	-1.76185500
C	1.47762600	1.66353000	-0.66425000
C	2.56074100	2.49231000	-0.95218400
C	3.22847100	3.12583200	0.09338600
C	2.79660400	2.90342800	1.40107700
C	1.71679600	2.05453700	1.61140500
N	-0.04406300	-0.21000100	-1.24341700
N	-1.79198800	-1.32608300	0.47232200
N	-1.76968900	1.39889100	-0.01053300
N	1.06152600	1.45563700	0.60199200
N	-0.81724900	0.39560000	2.47817900
O	-1.29450200	-0.08911400	3.42978700
H	3.96037800	-1.55778900	1.75271700
H	5.80771500	-1.64859600	0.10741100
H	5.30899500	-1.60732800	-2.33605000
H	2.95308400	-1.50529100	-3.09971300
H	0.66870400	-1.59296800	-2.68841500
H	0.15275600	-2.29970900	-1.13863000
H	-1.59944900	-0.47448700	-2.73852300
H	-3.22857400	-2.38635900	-2.39327600
H	-4.21623700	-4.05436800	-0.80346900
H	-3.58570400	-3.92290600	1.62440400
H	-1.99382300	-2.14382200	2.35833600

H	-3.35210000	1.38886300	-2.99161200
H	-4.35649900	3.46301400	-2.00532700
H	-3.64145600	4.17441700	0.29444400
H	-1.95220000	2.78197700	1.51039800
H	1.33792600	0.70938000	-2.58893800
H	-0.04763900	1.70333100	-2.16286700
H	2.87881900	2.62683500	-1.98117700
H	4.07653700	3.77283200	-0.10850600
H	3.29149400	3.36528700	2.24829900
H	1.35581200	1.82938200	2.60871700

BP86:

Fe	10.11863800	2.42173000	3.57876200
S	9.39360400	4.40427300	4.55084600
C	7.69967700	4.14492200	5.01270400
C	7.25415900	4.59998100	6.27549000
C	5.90785100	4.48095500	6.64601500
C	4.98035800	3.88194400	5.77577000
C	5.41249300	3.41691800	4.52550100
C	6.75754600	3.54981700	4.12863600
C	7.19345600	3.11949200	2.75397200
C	8.67705000	1.64079100	1.40242100
C	9.45849800	2.85480200	0.91277700
C	9.37812700	3.40077100	-0.37124200
C	10.20082100	4.49217300	-0.69338600
C	11.06961500	4.99714800	0.28554100
C	11.09025500	4.40840100	1.55504800
C	9.68051300	0.50899700	1.55076900
C	9.78747300	-0.60949700	0.71848900
C	10.81622000	-1.53380600	0.96602000
C	11.69318100	-1.30408000	2.03849200
C	11.51635000	-0.16606500	2.83393200
C	7.64262400	0.82166900	3.55778300
C	8.19879600	0.80715400	4.97121300
C	7.54595300	0.14779300	6.02122100
C	8.14193900	0.11629900	7.28897300
C	9.37780300	0.75535600	7.46965100
C	9.96705300	1.40489800	6.38172900
N	8.18589900	1.98259800	2.78744500
N	10.30668700	3.34835700	1.86267500
N	10.52828200	0.72693600	2.59398400
N	9.39894300	1.42328000	5.15175700
N	11.69581400	2.73596200	4.16453200
O	12.59717500	3.51119400	4.13460400
H	7.97815900	5.05679900	6.95812300
H	5.58261400	4.85120000	7.62442900

H	3.92917800	3.78419200	6.06550400
H	4.69095300	2.96742700	3.83079400
H	6.31941900	2.80133200	2.14997500
H	7.69492100	3.95703700	2.23638600
H	7.85553200	1.37854200	0.70823000
H	8.67718300	2.98310300	-1.10064600
H	10.15579200	4.94438700	-1.68884500
H	11.72338800	5.84935600	0.08058100
H	11.74226200	4.77564000	2.35323400
H	9.08134000	-0.75294800	-0.10543200
H	10.92913300	-2.41880800	0.33232500
H	12.50924600	-1.99683700	2.26247700
H	12.16801200	0.06152100	3.68291700
H	6.53872400	0.85095800	3.57971300
H	7.93154000	-0.11500500	3.04832200
H	6.57602500	-0.32682600	5.84205800
H	7.64571200	-0.39062900	8.12245400
H	9.87933700	0.76707100	8.44132000
H	10.91787900	1.93792300	6.46975400

References

(1) Schopfer, M. P.; Mondal, B.; Lee, D. H.; Sarjeant, A. A. N.; Karlin, K. D. *J. Am. Chem. Soc.* **2009**, *131*, 11304.
(2) McQuilken, A. C.; Jiang, Y. B.; Siegler, M. A.; Goldberg, D. P. *J. Am. Chem. Soc.* **2012**, *134*, 8758.
(3) Lubben, M.; Meetsma, A.; Wilkinson, E. C.; Feringa, B.; Que, L., Jr. *Angew. Chem., Int. Ed.* **1995**, *34*, 1512.
(4) Sheldrick, G. M. *Acta Cryst. A* **2008**, *64*, 112.
(5) Solomon, E. I.; Hedman, B.; Hodgson, K. O.; Dey, A.; Szilagyi, R. K. *Coord. Chem. Rev.* **2005**, *249*, 97.
(6) George, G. N.; Stanford Synchrotron Radiaton Laboratory: Menlo Park, CA, 1990.
(7) Tenderholt, A. L.; v2.1, Ed.; Stanford University: Stanford, CA, 2007.
(8) Sarangi, R.; George, S. D.; Rudd, D. J.; Szilagyi, R. K.; Ribas, X.; Rovira, C.; Almeida, M.; Hodgson, K. O.; Hedman, B.; Solomon, E. I. *J. Am. Chem. Soc.* **2007**, *129*, 2316.
(9) Frisch, M. J.; Trucks, G. W.; Schlegel, H. B.; Scuseria, G. E.; Robb, M. A.; Cheeseman, J. R.; Scalmani, G.; Barone, V.; Mennucci, B.; Petersson, G. A.; Nakatsuji, H.; Caricato, M.; Li, X.; Hratchian, H. P.; Izmaylov, A. F.; Bloino, J.; Zheng, G.; Sonnenberg, J. L.; Hada, M.; Ehara, M.; Toyota, K.; Fukuda, R.; Hasegawa, J.; Ishida, M.; Nakajima, T.; Honda, Y.; Kitao, O.; Nakai, H.; Vreven, T.; Montgomery, J. A.; Peralta, J. E.; Ogliaro, F.; Bearpark, M.; Heyd, J. J.; Brothers, E.; Kudin, K. N.; Staroverov, V. N.; Kobayashi, R.; Normand, J.; Raghavachari, K.; Rendell, A.; Burant, J. C.; Iyengar, S. S.; Tomasi, J.; Cossi, M.; Rega, N.; Millam, J. M.; Klene, M.; Knox, J. E.; Cross, J. B.; Bakken, V.; Adamo, C.; Jaramillo, J.; Gomperts, R.; Stratmann, R. E.; Yazyev, O.; Austin, A. J.; Cammi, R.; Pomelli, C.; Ochterski, J. W.; Martin, R. L.; Morokuma, K.; Zakrzewski, V. G.; Voth, G. A.; Salvador, P.; Dannenberg, J. J.; Dapprich, S.; Daniels, A. D.; Farkas; Foresman, J. B.; Ortiz, J. V.; Cioslowski, J.; Fox, D. J. Wallingford CT, 2009.
(10) Neese, F. *Inorg. Chim. Acta* **2002**, *337*, 181.
(11) Sinnecker, S.; Slep, L. D.; Bill, E.; Neese, F. *Inorg. Chem.* **2005**, *44*, 2245.